Weak-conjugation linked donor-acceptor emitters for efficient near-ultraviolet organic light-emitting diodes with narrowed full width at half maximum

Ziting Zhong,[a,‡] Zhangshan Liu,[b,‡] Xianhui Wang,[a] Dan Xiong,[a] Huihui Li,[a] Xin Jiang Feng,*[,a] Zujin Zhao,*[,b] and Hua Lu*[,a]

I. Supplementary Figures and Tables.

I. Supplementary Figures and Tables.

Table S1 Crystal data and structure refinement for mo220117a.

Identification code	mo220117a
Empirical formula	$C_{49}H_{37}N_3$
Formula weight	667.81
Temperature/K	296.15
Crystal system	orthorhombic
Space group	$P2_12_12_1$
a/Å	10.1481(8)
b/Å	14.2647(10)
c/Å	24.5582(18)
α/°	90
β/°	90
γ/°	90
Volume/Å^3	3555.0(5)
Z	4
ρ_{calc}g/cm^3	1.248
μ/mm^{-1}	0.073
F(000)	1408.0
Crystal size/mm^3	0.15 × 0.12 × 0.12
Radiation	MoKα (λ = 0.71073)
2Θ range for data collection/°	3.302 to 60.822
Index ranges	-14 ≤ h ≤ 14, -20 ≤ k ≤ 17, -34 ≤ l ≤ 34
Reflections collected	38727
Independent reflections	10044 [R_{int} = 0.0610, R_{sigma} = 0.0686]
Data/restraints/parameters	10044/0/472
Goodness-of-fit on F^2	1.001
Final R indexes [I>=2σ (I)]	R_1 = 0.0501, wR_2 = 0.0916
Final R indexes [all data]	R_1 = 0.1060, wR_2 = 0.1098
Largest diff. peak/hole / e Å^{-3}	0.13/-0.14
Flack parameter	-0.7(10)

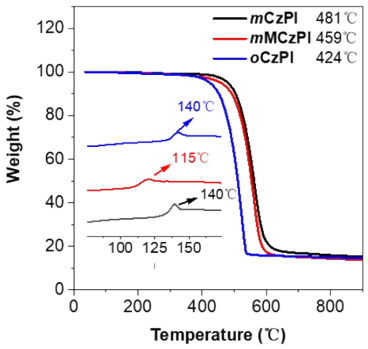

Fig. S1 Thermogravic analysis (TGA) traces for ***m*CzPI**, ***m*MCzPI**, and ***o*CzPI**. Inset: differential scanning calorimetry (DSC) traces.

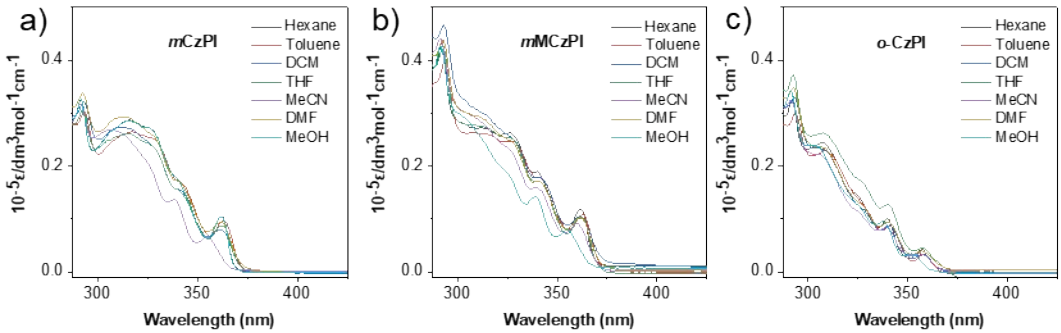

Fig. S2 Absorption spectra of ***m*CzPI**(a), ***m*MCzPI**(b) and ***o*CzPI**(c) in different solvents.

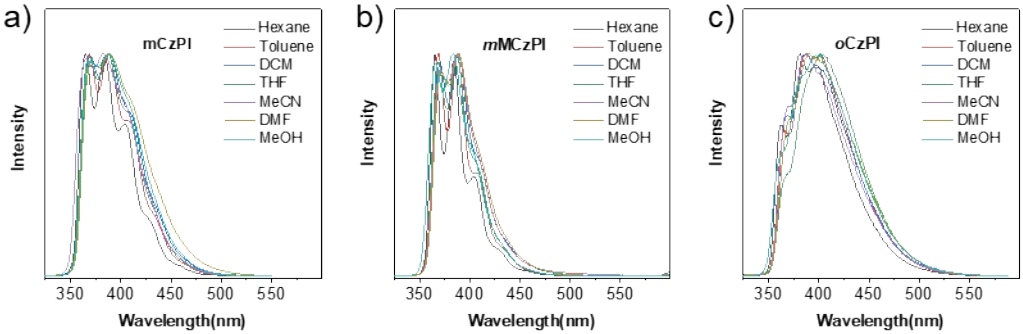

Fig. S3 Emission spectra of ***m*CzPI**(a), ***m*MCzPI**(b) and ***o*CzPI**(c) in different solvents.

Table S2 Photophysical properties of ***m*CzPI**, ***m*MCzPI**, and ***o*CzPI** in different solvents.

	Solvent	λ_{abs} [a] (nm)	ε_{abs} [b] (M cm^{-1})	λ_{em} [a] (nm)	$\Delta\nu_{em\text{-}abs}$ [c](cm^{-1})	Φ_F [d]	τ_F (ns)[e]
***m*CzPI**	Hexane	317	32700	364	4073	0.47	4.0
	Toluene	318	30400	369	4346	0.62	3.9
	DCM	312	32200	389	6344	0.58	5.8
	THF	315	30600	387	5906	0.37	5.6
	MeCN	308	31700	383	6358	0.56	5.1
	DMF	314	33800	389	6140	0.50	6.5
	MeOH	310	32600	387	6418	0.53	5.1
***m*MCzPI**	Hexane	327	42700	365	3184	0.43	4.4
	Toluene	328	43700	368	3314	0.27	4.1
	DCM	327	39700	388	4808	0.54	4.6
	THF	326	46700	385	4701	0.19	5.3
	MeCN	324	42700	388	5091	0.53	4.7
	DMF	327	44100	388	4808	0.44	8.5
	MeOH	325	44000	383	4660	0.52	4.8
***o*CzPI**	Hexane	308	34000	382	6290	0.21	2.3
	Toluene	309	32500	386	6456	0.15	2.7
	DCM	308	30000	388	6694	0.29	3.4
	THF	308	33100	402	7591	0.15	3.5
	MeCN	306	37200	388	6907	0.22	3.0
	DMF	306	32400	390	7039	0.22	3.6
	MeOH	304	34900	401	7957	0.32	3.1

[a] Absorption and emission maxima. [b] Molar absorption coefficients measured in solution. [c] Stokes-shift value. [d] Fluorescence quantum yield. [e] Fluorescence lifetime detected at the maximum fluorescence wavelengths.

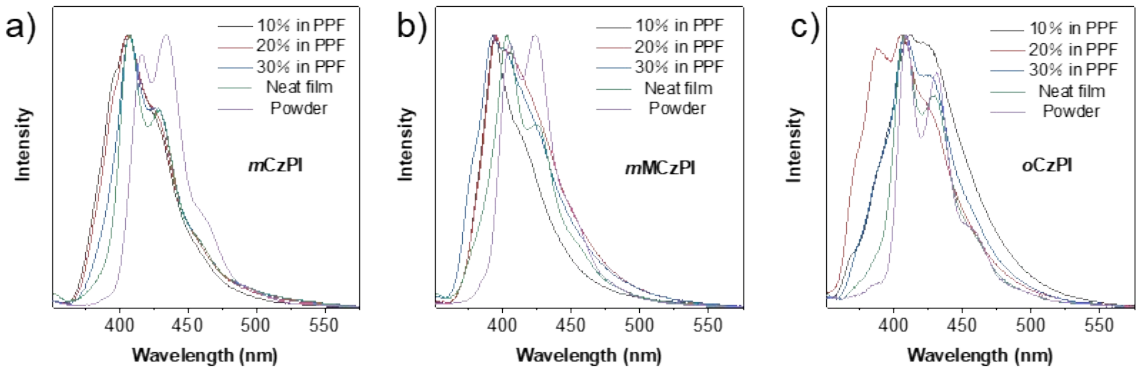

Fig. S4 Emission spectra of a) ***m*CzPI**, b) ***m*MCzPI** and c) ***o*CzPI** in film and in powder.

Table S3 Emission band maxima and the absolute quantum yields of ***m*CzPI**, ***m*MCzPI**, and ***o*CzPI** in PPF film and the powder form.

E_m/Φ_F	Film				Powder
	10% in PPF	20% in PPF	30% in PPF	Neat	
***m*CzPI**	406/0.60	406/0.50	408/0.42	406/0.33	433/0.51
***m*MCzPI**	394/0.45	395/0.55	393/0.49	403/0.31	423/0.51
***o*CzPI**	412/0.61	405/0.50	408/0.48	408/0.32	408/0.61

PPF = 2,8-bis(diphenylphosphoryl)dibenzo[b,d]furan

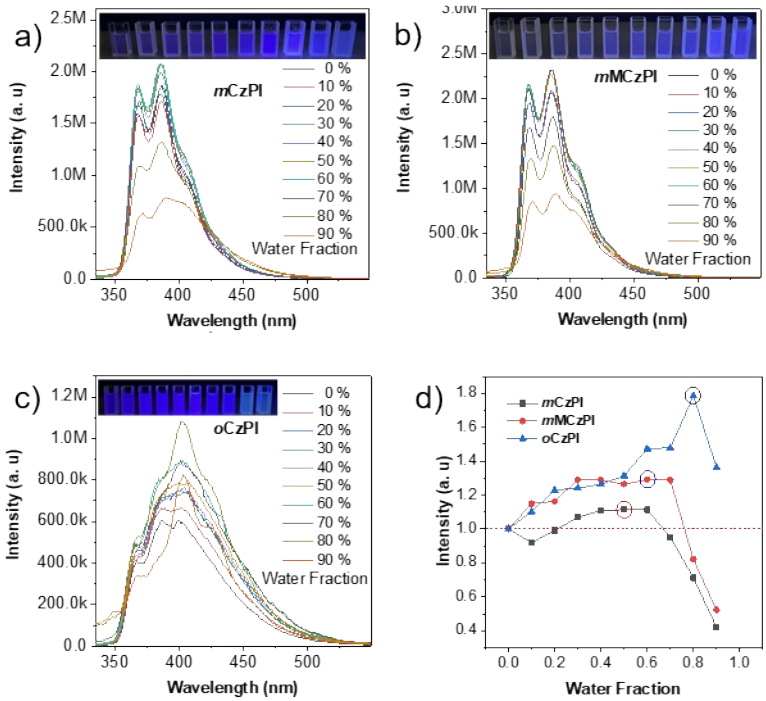

Fig. S5 Emission spectra and intensity for a) ***m*CzPI**, b) ***m*MCzPI**, c) ***o*CzPI** with different water fractions in THF/H_2O and d) the relative intensity comparison with different water fractions..

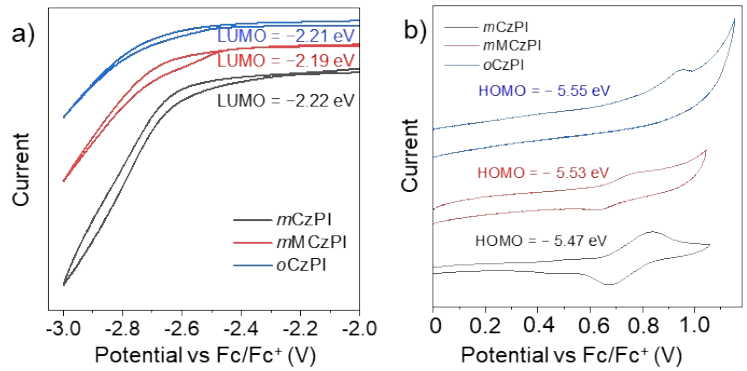

Fig. S6 Cyclic voltammograms curves of ***m*CzPI**, ***m*MCzPI**, and ***o*CzPI** measured in a) DMF for reduction and b) CH_2Cl_2 for oxidation versus Fc/Fc^+.

Table S4 Calculated excited wavelength (λ), oscillator strengths (*f*) and the related wave functions calculated by using the B3LYP functional with 6-31G(d,p) basis sets by TDDFT method in the gas phase.

	State[a]	E (eV) [b]	λ(nm)[c]	*f* [d]	Orbital (coefficient)[e]
***m*CzPI**	S_1	3.63	342	0.6084	H-1→L (56%), H→L (31%)
	S_2	3.71	335	0.0863	H-1→L (28%), H→L (54%)
	S_3	3.77	329	0.0581	H→L+1 (51%), H→L+2 (29%)
	S_4	3.83	324	0.0211	H→L+1 (39%), H→L+2 (38%)
	S_5	3.96	313	0.0656	H-1→L (11%), H-1→L+1 (65%)
	S_6	4.01	310	0.0611	H-1→L+3 (78%), H→L+3 (13%)
	S_7	4.04	307	0.0288	H→L+4 (82%)
	S_8	4.09	304	0.0335	H-3→L (19%), H→L+5 (50%)
	S_{10}	4.22	295	0.0331	H-1→L+2 (14%), H→L+6 (53%)
***m*MCzPI**	S_1	3.72	334	0.495	H-1→L (56%), H→L (32%)
	S_2	3.77	330	0.1417	H-1→L (26%), H→L (62%)
	S_3	3.87	321	0.0722	H-1→L+1 (71%)
	S_4	4.01	310	0.0318	H-3→L (10%), H-1→L+1 (14%), H-1→L+2 (53%)
	S_5	4.05	307	0.1483	H→L+1 (27%), H→L+2 (40%)
	S_6	4.07	305	0.0432	H→L+4 (86%)
***o*CzPI**	S_1	3.66	339	0.2095	H→L (90%)
	S_2	3.82	325	0.1516	H-1→L (83%)
	S_4	4.06	306	0.0543	H→L+4 (87%)
	S_6	4.11	302	0.0857	H-1→L+2 (16%), H→L+1 (17%), H→L+3 (53%)
	S_8	4.21	295	0.0206	H-1→L+2 (30%), H-1→L+3 (44%), H→L+2 (12%)
	S_{10}	4.24	293	0.0335	H-3→L (18%), H-1→L+1 (10%), H-1→L+5 (38%), H→L+5 (18%)

[a] Excited state. [b] Calculated energy gaps. [c] Experimental absorption wavelengths [d] Oscillator strength (values < 0.02 are not included). [e] MOs involved in the transitions, H = HOMO, L = LUMO.

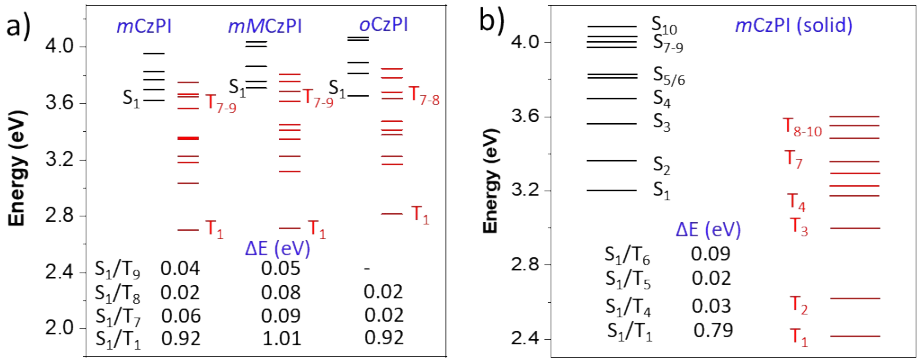

Fig. S7 Singlet and triplet excited states calculated by B3LYP/6-31G(d,p) by TDDFT method for ***m*CzPI**, ***m*MCzPI**, and ***o*CzPI** in the gas phase a) and by QM/MM method for ***m*CzPI** in the solid state b).

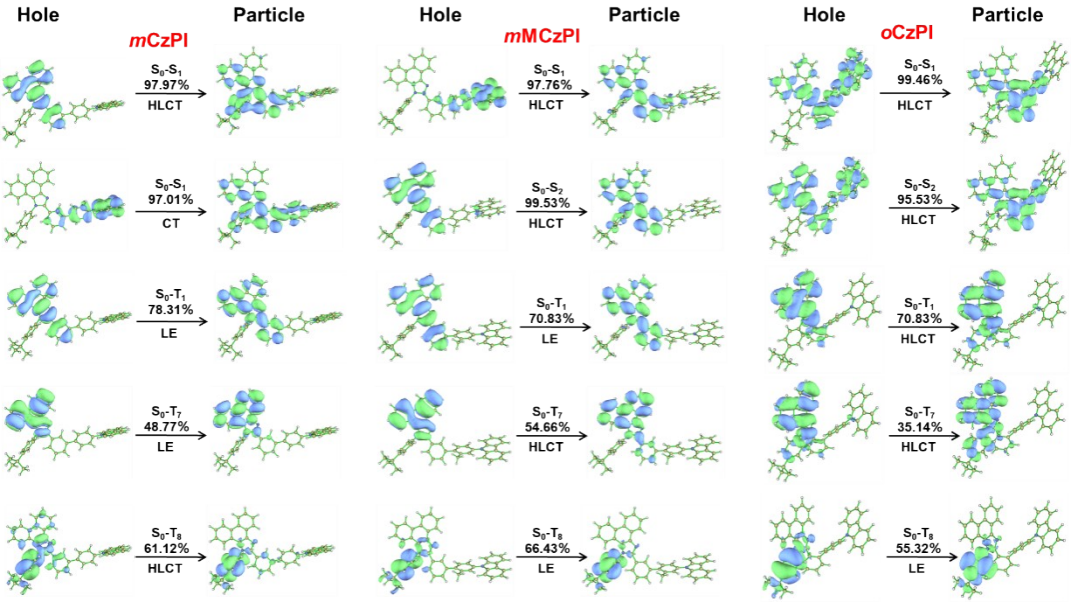

Fig. S8 Natural transition orbitals for S_0 to S_n/T_n for ***m*CzPI**, ***m*MCzPI**, and ***o*CzPI**. The isosurface value is 0.02 au.

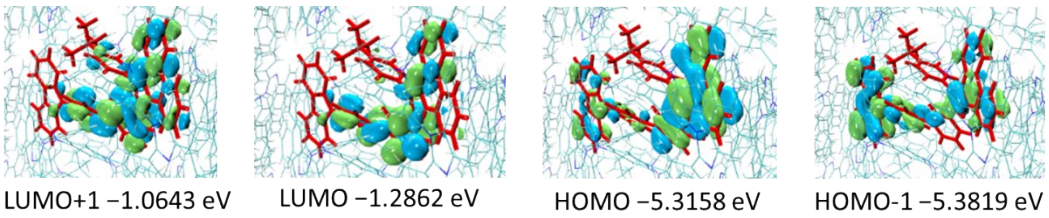

Fig. S9 Frontier molecular orbital diagrams for ***m*CzPI** with B3LYP/6-31G(d,p) by QM/MM method (HOMO−1, HOMO, LUMO, LUMO+1 from right to left). The isosurface value is 0.02 au.

Table S5 Calculated excited wavelength (λ), oscillator strengths (*f*) and the related wave functions calculated by using the B3LYP functional with 6-31G(d,p) basis sets by QM/MM method.

State[a]	E (eV) [b]	λ(nm)[c]	*f* [d]	Orbital (coefficient)[e]

***m*CzPI**	S_1	3.20	387	0.0920	H-1→L (9%), H→L (89%)
	S_2	3.36	369	0.5869	H-1→L (90%), H→L+1 (11%)
	S_3	3.56	348	0.2433	H-1→L (9%), H→L+1 (79%)
	S_6	3.83	323	0.0273	H-1→L+1 (91%)
	S_7	3.98	311	0.0669	H-1→L+3 (78%), H→L+3 (10%)
	S_8	3.99	310	0.0354	H-3→L (21%), H→L+4 (64%)
	S_9	4.03	308	0.0721	H-3→L (51%), H→L+4 (13%), H→L+5 (16%), H→L+6 (13%)

[a] Excited state. [b] Calculated energy gaps. [c] Experimental absorption wavelengths [d] Oscillator strength (values < 0.02 are not included). [e] MOs involved in the transitions, H = HOMO, L = LUMO.

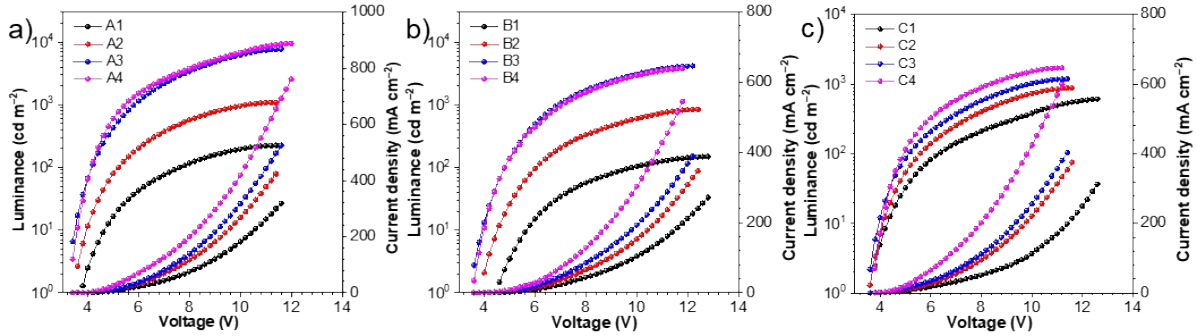

Fig. S10 Luminance-voltage-current density characteristics for devices using a) ***m*CzPI**, b) ***m*MCzPI**, and c) ***o*CzPI** as emitters.

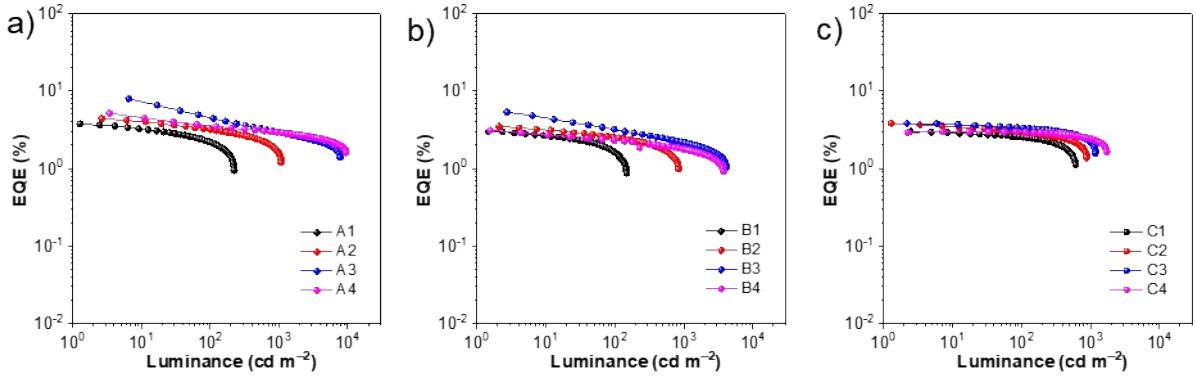

Fig. S11 External quantum efficiencies (EQE)-luminance characteristics for devices using a) ***m*CzPI**, b) ***m*MCzPI**, and c) ***o*CzPI** as emitters.

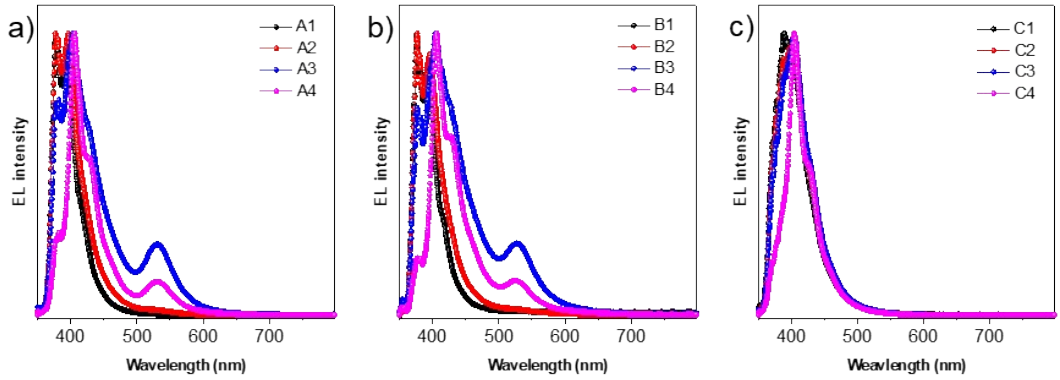

Fig. S12 EL spectra for devices using a) ***m*CzPI**, b) ***m*MCzPI**, and c) ***o*CzPI** as emitters.

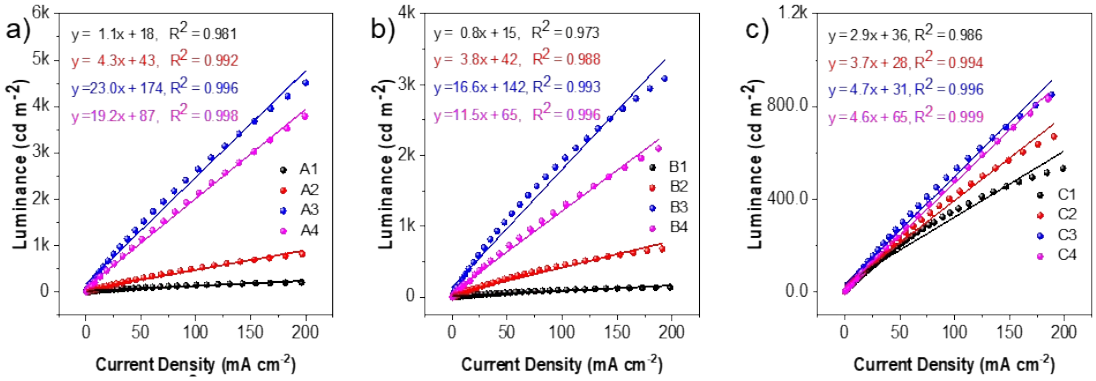

Fig. S13 Luminance versus current density (symbol) and the fitted curve plot (line) of devices.

Table S6 EL performance of devices using ***m*CzPI**, ***m*MCzPI**, and ***o*CzPI** as emitters.

Device [e]	λ_{EL} (nm)	V [a] (V)	L [b] (cd m^{-2})	η_c [b] (cd A^{-1})	η_P [b] (lm W^{-1})	η_{ext} [b] (%)	η_r (%) [c]	CIE (x, y) [d]
				maximum value / at 100 cd m^{-2}				
A1	376/395	3.7	223.5	0.28/0.16	0.23/0.07	3.78/2.20	21−32%	(0.165, 0.028)
A2	377/396	3.5	1079	0.95/0.68	0.83/0.41	4.45/3.17	30−45%	(0.166, 0.062)
A3	404	3.3	7730	8.47/4.71	7.82/3.52	7.97/4.43	62−93%	(0.185, 0.199)
A4	406	3.3	9417	3.99/2.70	3.68/2.02	5.17/3.50	37−56%	(0.178, 0.144)
B1	376/393	4.5	148.5	0.19/0.10	0.13/0.03	3.03/1.64	22−34%	(0.166, 0.027)
B2	376/395	3.9	839.2	0.87/0.62	0.68/0.33	3.53/2.54	21−32%	(0.170, 0.072)
B3	404	3.5	4146	5.54/2.23	4.83/1.00	5.34/2.15	36−54%	(0.183, 0.184)
B4	406	3.5	3739	2.35/1.35	2.05/0.61	3.13/1.80	34−50%	(0.176, 0.130)
C1	388	3.7	612.5	0.58/0.44	0.44/0.22	3.04/2.54	17−25%	(0.163, 0.045)
C2	404	3.5	878.3	0.66/0.51	0.58/0.29	3.85/2.97	26−39%	(0.162, 0.042)
C3	404	3.5	1183	0.71/0.62	0.62/0.38	3.83/3.35	27−40%	(0.162, 0.043)
C4	404	3.7	1718	0.53/0.52	0.43/0.33	2.99/2.93	31−47%	(0.162, 0.037)

[a] Turn-on voltage at 1 cd m^{-2}. [b] The luminance (L), current efficiency (η_c), power efficiency (η_P) and external quantum efficiency (η_{ext}) of the devices: maximum values/ values at 100 cd m^{-2}. [c] Exciton utility efficiency (η_r), calculated by $\eta_{ext} = \gamma \times \eta_{PL} \times \eta_r \times \eta_{out}$, in which γ is a balance factor of carriers (100%), η_{PL} is the film fluorescent efficiencies, and η_{out} stands for the light extraction rate (0.25 ± 0.05 for ITO glass substrate). [d] CIE coordinates at 100 cd/m^2. [e] Device configurations and the functional materials used are as follows:

ITO/HATCN(5 nm)/TAPC(50 nm)/TcTa(5 nm)/mCP (5 nm)/EML(20 nm)/PPF(5 nm)/TmPyPB(30 nm)/LiF(1 nm)/Al

A1: EML = 10% *m*CzPI: PPF

A2: EML = 20% *m*CzPI: PPF

A3: EML = 30% *m*CzPI: PPF

A4: EML = *m*CzPI

B1: EML = 10% *m*MCzPI: PPF

B2: EML = 20% *m*MCzPI: PPF

B3: EML = 30% *m*MCzPI: PPF

B4: EML = *m*MCzPI

C1: EML = 10% *o*MCPI: PPF

C2: EML = 20% *o*MCPI: PPF

C3: EML = 30% *o*MCPI: PPF

C4: EML = *o*MCPI

Indium tin oxide (ITO) is transparent an anode; dipyrazino[2,3-f:2′,3′-h]quinoxaline-2,3,6,7,10,11-hexacarbonitrile (HATCN) is applied as a hole injection layer; 4,4′-cyclohexylidenebis[*N*,*N*-bis(4-methylphenyl)aniline] (TAPC) is a hole-transporting layer; tris[4-(carbazol-9-yl)phenyl]amine (TCTA) functions not only as a hole-transporting layer but also an electron-blocking layer; 1,3-bis(carbazol-9-yl)benzene (mCP) works as a buffer layer between hole-transporting layer and EML; (2,8-bis(diphenylphosphoryl)dibenzo[b,d]furan) (PPF) is used as an exciton blocking layer and host in doped devices; 1,3,5-tri(m-pyrid-3-yl-phenyl)benzene (TmPyPB) is utilized as an electron-transporting layer, and LiF/Al works as a cathode.

II. Measurements

Photophysical, thermal and electrochemical property measurements

^{1}H and ^{13}C NMR spectra were recorded on a Bruker AM 400/500 spectrometer. Mass spectrometric measurements were recorded using a MicroQII mass spectrometer. The differential scanning calorimetry (DSC) analysis was performed with 10 ^{o}C min^{-1} heating rate under nitrogen flushing using a TA Instruments DSC 2920. Thermogravimetric analysis was undertaken using a TGA instrument (PE-TGA6) with 20 ^{o}C min^{-1} heating rate under nitrogen. UV-Vis spectra were recorded using a Shimadzu UV-1800 spectrophotometer. Samples for absorption and emission measurements were contained in 1×1 cm quartz cuvettes. Dilute solution with an absorbance of less than 0.05 at the excited wavelength was used for the measurement of fluorescent quantum yields, and the absolutely quantum yields of the materials were determined with a Hamamatsu C13534 spectrometer. Cyclic voltammetric (CV) measurements were carried out in a conventional three-electrode cell, using a Pt button working electrode, a platinum wire counter electrode, and an $Ag/AgNO_3$ reference electrode using a computer-controlled CHI650E at room temperature in dichloromethane (for oxidation) or dimethylformamide (for reduction) containing Bu_4NPF_6 (0.1 M) as the supporting electrolyte.

Single crystal structure measurement

Diffraction data were collected on a Bruker Smart Apex II CCD diffractometer or Bruker AXS Apex II diffractometer with graphite-monochromated Mo-Kα (λ = 0.71073 Å). An empirical (multi-scan) or numerical absorption correction was applied with the program SADABS. The structures were solved by direct method and subsequently refined on *F*2 by using full-matrix least-squares techniques (SHELXTL). The non-hydrogen atoms were refined anisotropically, and hydrogen atoms were located at calculated positions or found in the *F*map. A summary of the crystallographic data and selected experimental information are given in Table S1. The X-ray crystallographic coordinates for the structures reported in this article have been deposited at the Cambridge Crystallographic Data Centre (CCDC) under deposition numbers CCDC 2285450. These data can be obtained free of charge from The Cambridge Crystallographic Data Centre via www.ccdc.cam.ac.uk/data_request/cif.

Device fabrication and EL performance measurements

Glass substrates pre-coated with a 90 nm-thin layer of indium tin oxide (ITO) with a sheet resistance of 15−20 Ω per square were thoroughly cleaned for 10 minutes in ultrasonic bath of acetone, isopropyl alcohol, detergent, deionized water, and isopropyl alcohol and then treated with O_2 plasma for 10 min

in sequence. All of the organic materials used were purified by a vacuum sublimation approach. Organic layers were deposited onto the ITO-coated substrates by high-vacuum (< 5×10^{-4} Pa) thermal evaporation. Deposition rates were controlled by independent quartz crystal oscillators, which are 1~2 Å s^{-1} for organic materials, 0.1 Å s^{-1} for LiF, and 5 Å s^{-1} for Al, respectively. The emission area of the devices is 3 mm × 3 mm as shaped by the overlapping area of the anode and cathode. All the device characterization steps were carried out at room temperature under ambient laboratory conditions without encapsulation. EL spectra were taken by normal direction utilizing a spectrometer (Ocean Optics USB 2000+). Luminance−voltages− current density characteristics were measured by PIN-25D silicon photodiode, along with a Keithley 2400 Source Meter. The external quantum efficiencies were estimated utilizing the normalized EL spectra and the current efficiencies of the devices, assuming that the devices are Lambertian emitters.

III. ^{1}H NMR spectra of the compounds in $CDCl_3$

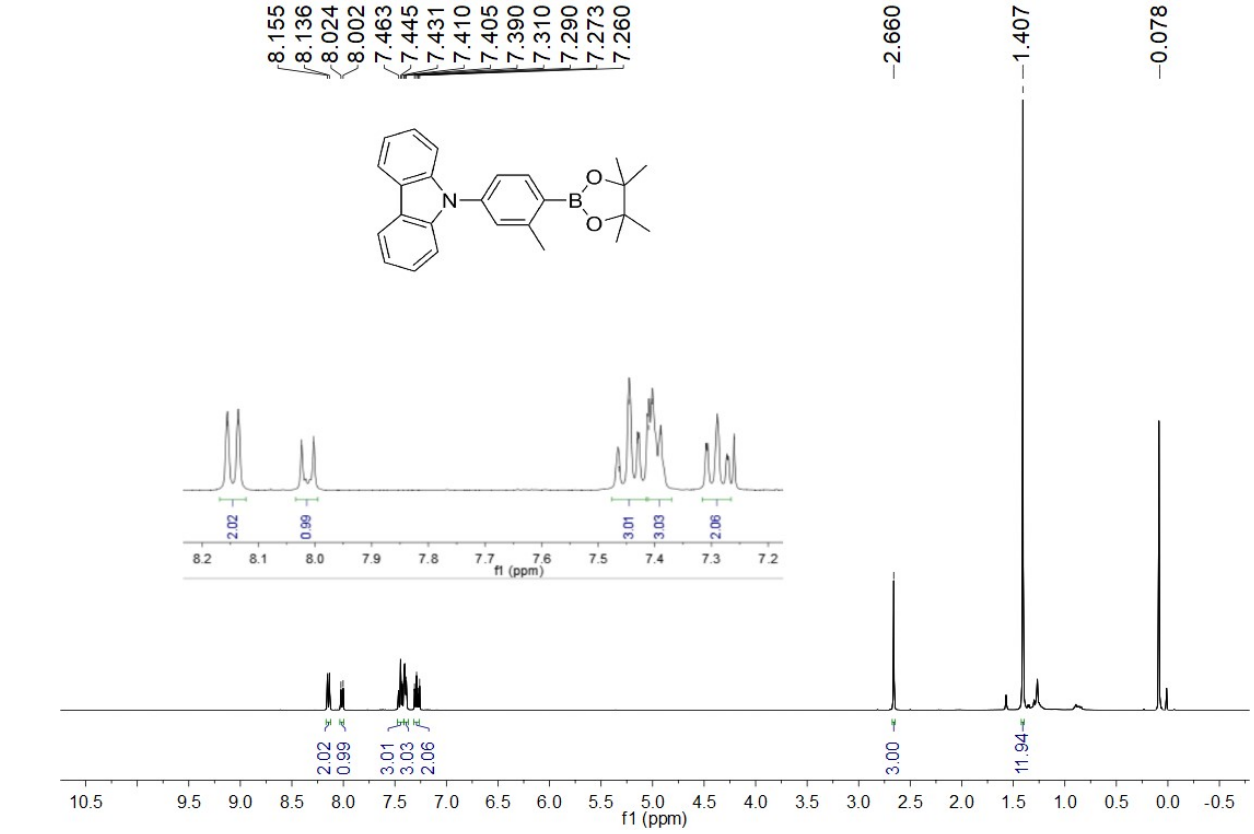

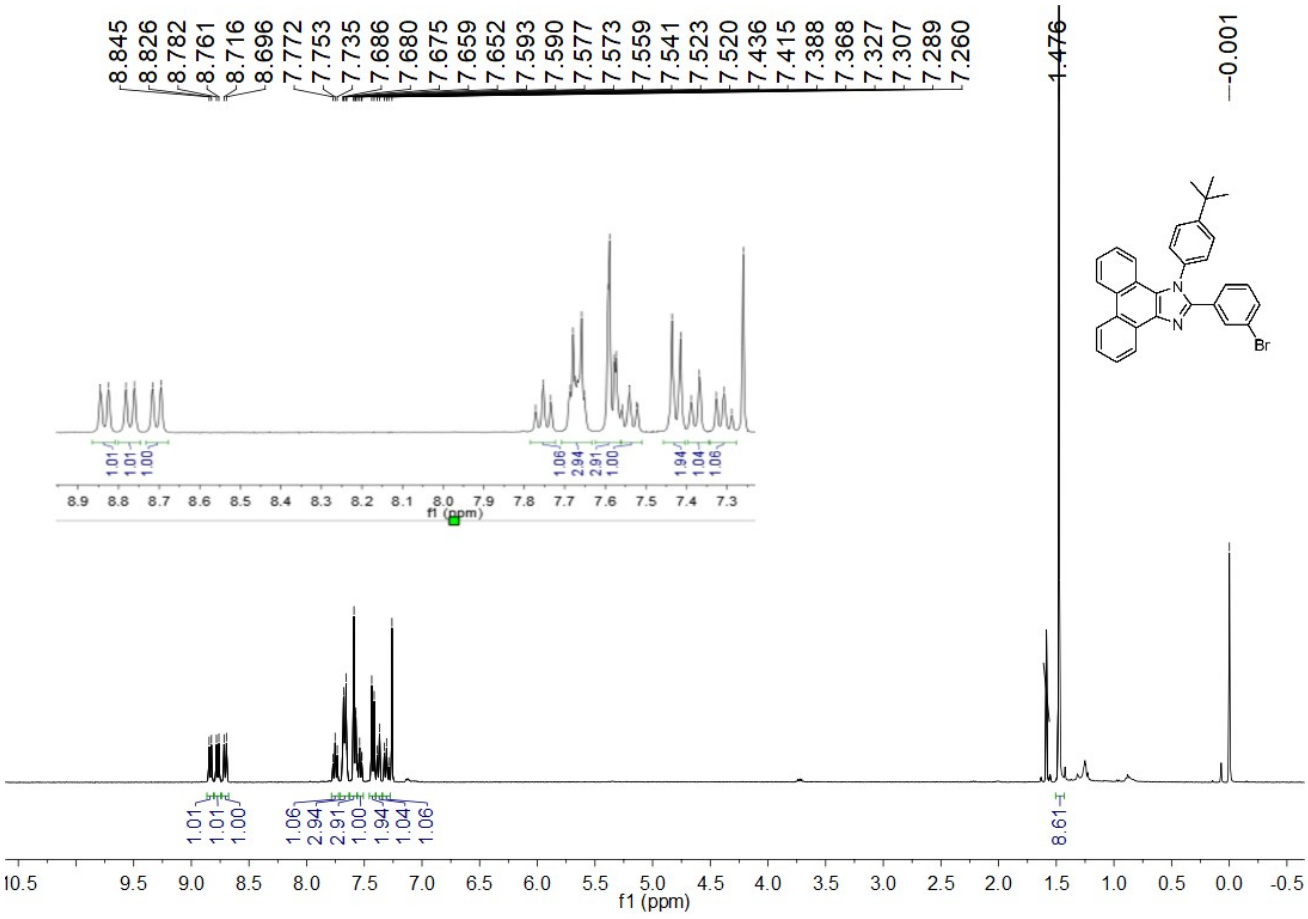

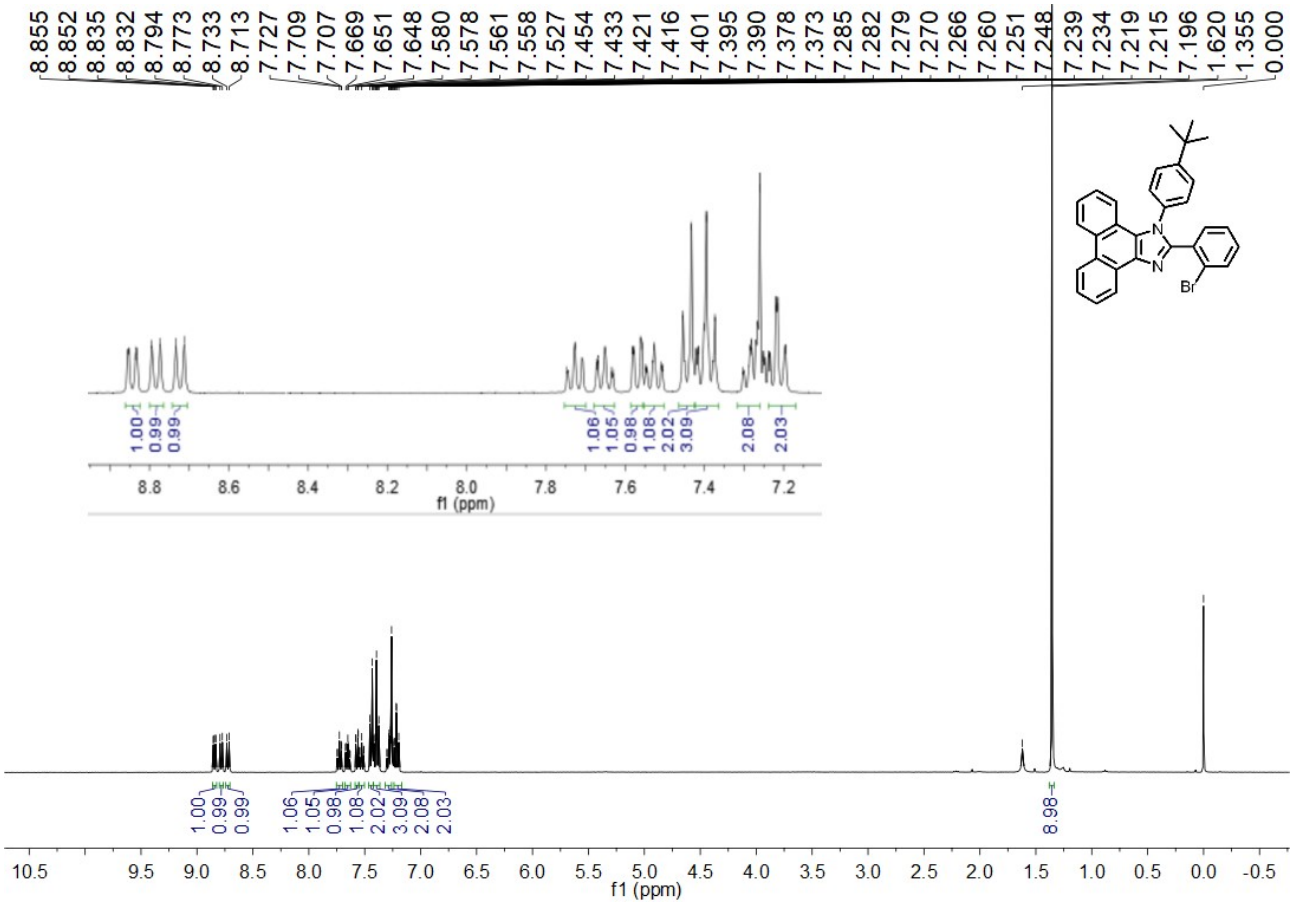
8.855
8.852
8.835
8.832
8.794
8.773
8.733
8.713
7.727
7.709
7.707
7.669
7.651
7.648
7.580
7.578
7.561
7.558
7.527
7.454
7.433
7.421
7.416
7.401
7.395
7.390
7.378
7.373
7.285
7.282
7.279
7.270
7.266
7.260
7.251
7.248
7.239
7.234
7.219
7.215
7.196
1.620
1.355
0.000
Br
f1 (ppm)
f1 (ppm)

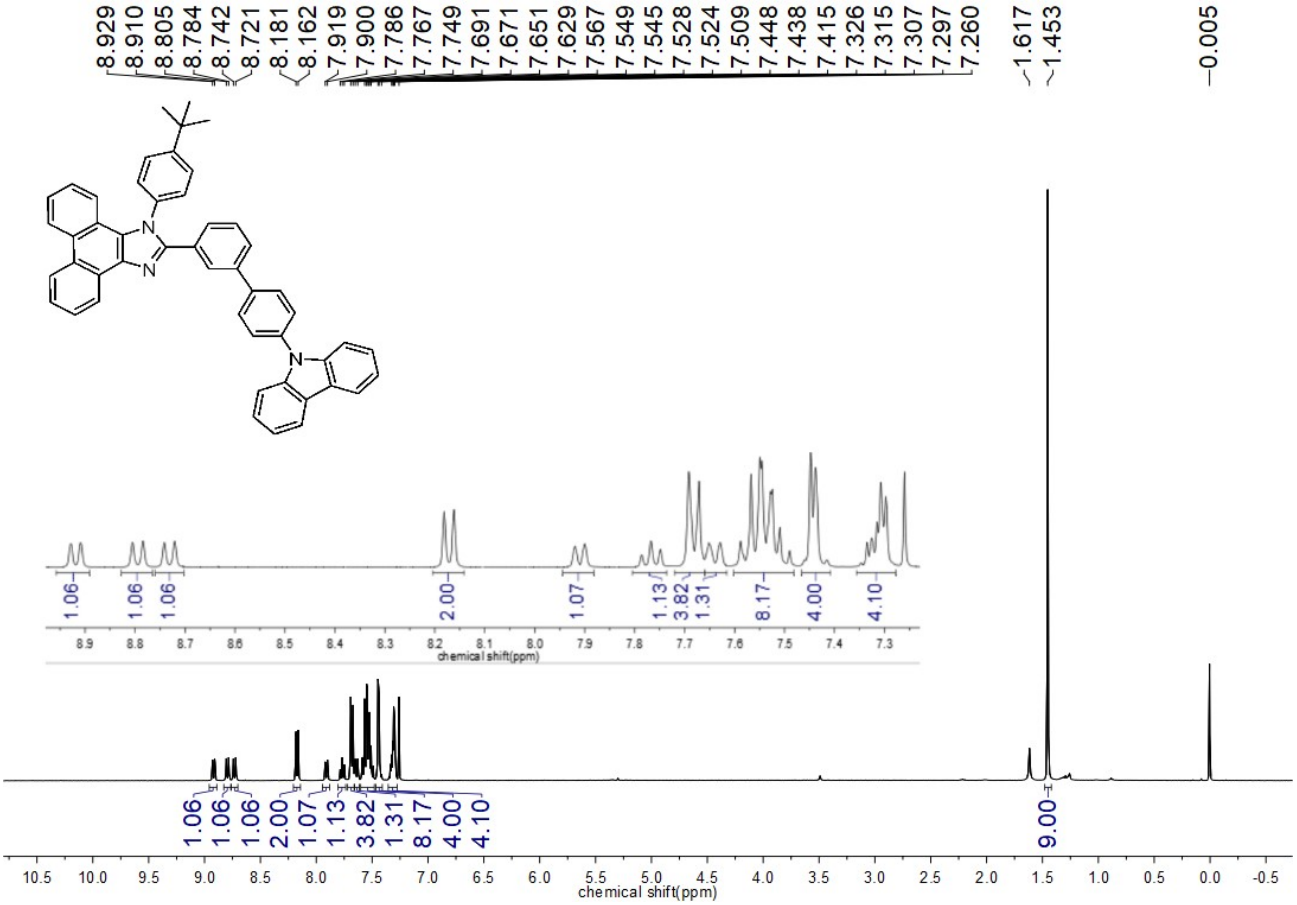
8.929
8.910
8.805
8.784
8.742
8.721
8.181
8.162
7.919
7.900
7.786
7.767
7.749
7.691
7.671
7.651
7.629
7.567
7.549
7.545
7.528
7.524
7.509
7.448
7.438
7.415
7.326
7.315
7.307
7.297
7.260
1.617
1.453
0.005
chemical shift(ppm)
chemical shift(ppm)

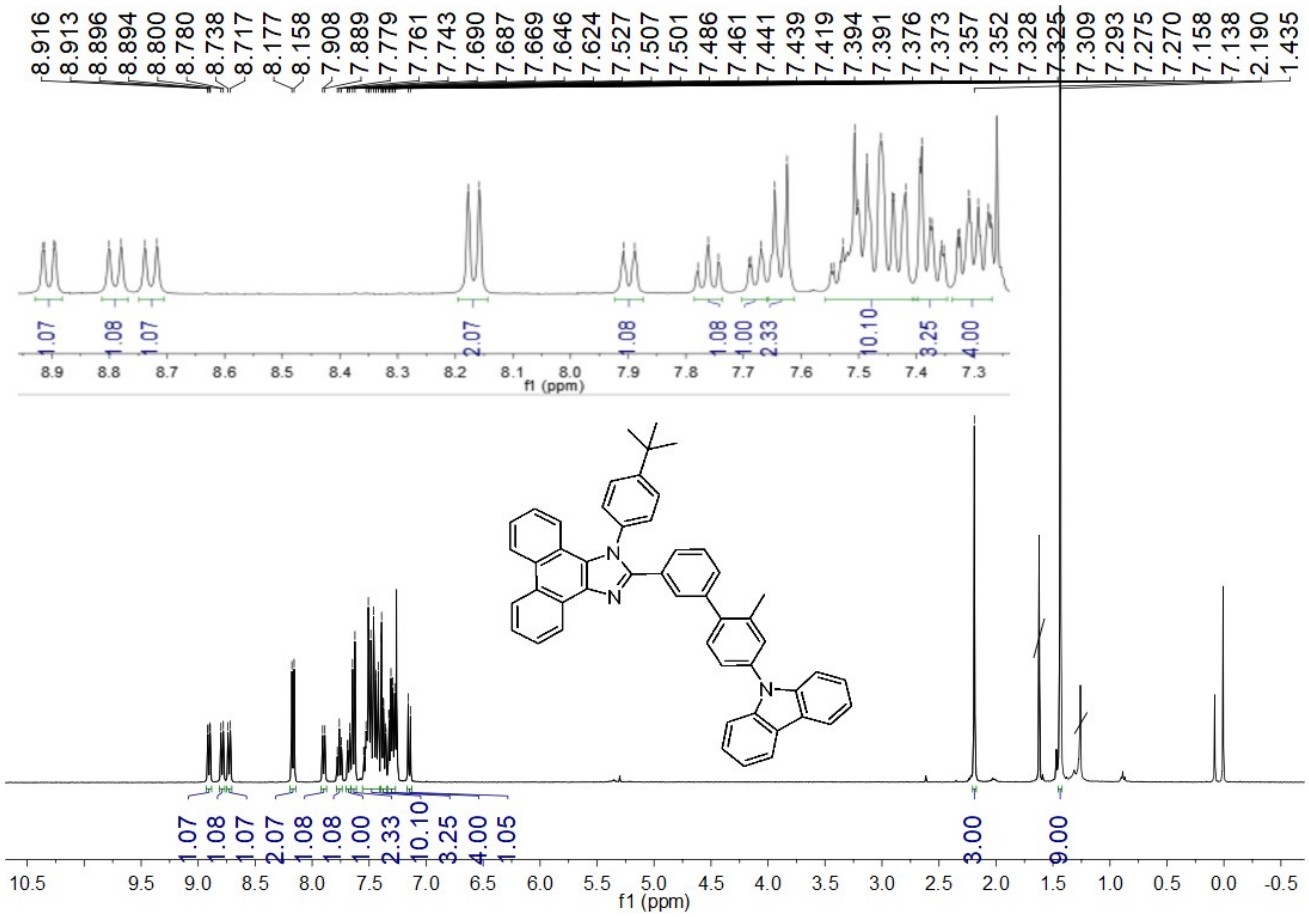
8.916
8.913
8.896
8.894
8.800
8.780
8.738
8.717
8.177
8.158
7.908
7.889
7.779
7.761
7.743
7.690
7.687
7.669
7.646
7.624
7.527
7.507
7.501
7.486
7.461
7.441
7.439
7.419
7.394
7.391
7.376
7.373
7.357
7.352
7.328
7.325
7.309
7.293
7.275
7.270
7.158
7.138
2.190
1.435
1.07
1.08
1.07
2.07
1.08
1.08
1.00
2.33
10.10
3.25
4.00
1.05
3.00
9.00
f1 (ppm)

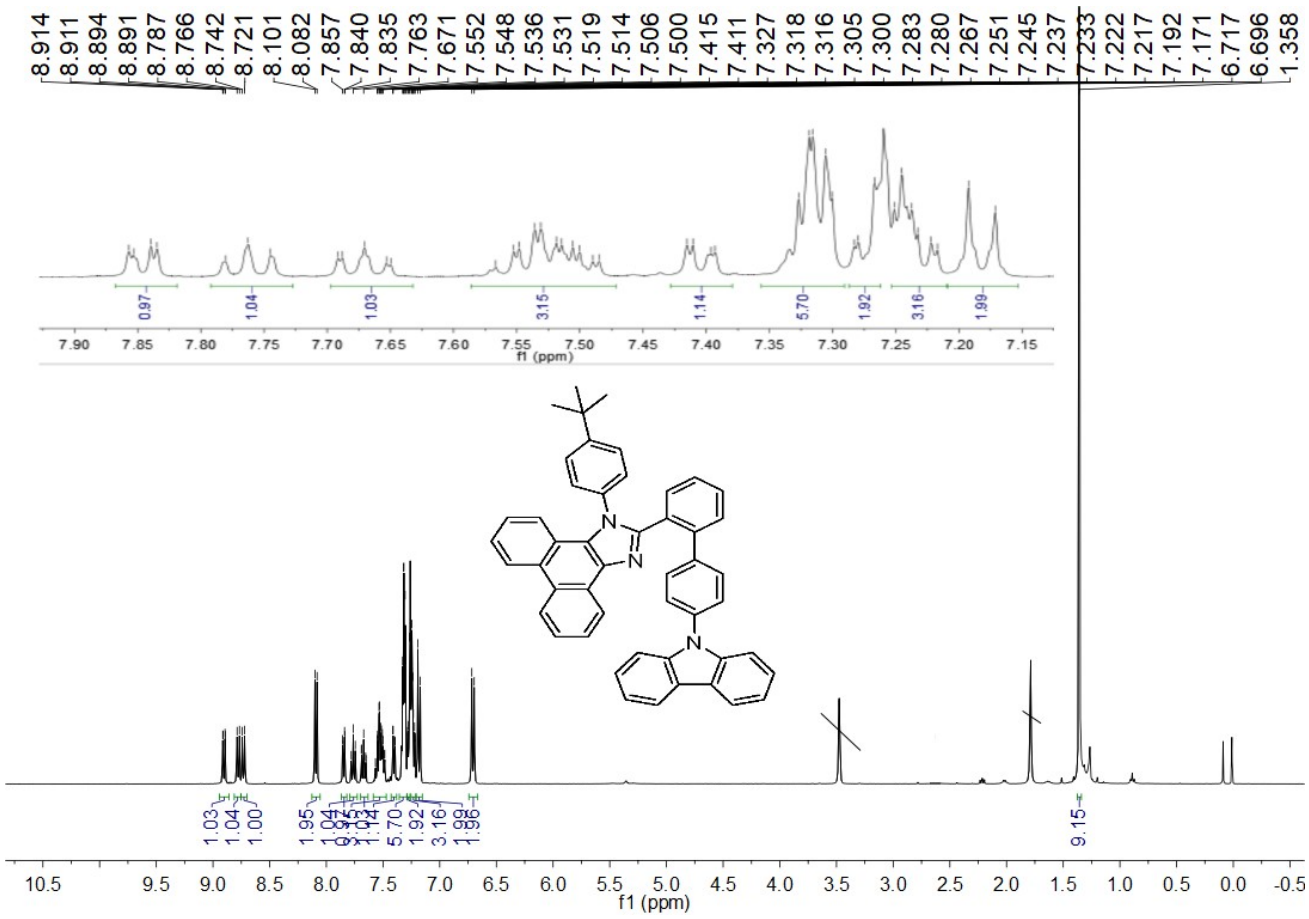
8.914
8.911
8.894
8.891
8.787
8.766
8.742
8.721
8.101
8.082
7.857
7.840
7.835
7.763
7.671
7.552
7.548
7.536
7.531
7.519
7.514
7.506
7.500
7.415
7.411
7.327
7.318
7.316
7.305
7.300
7.283
7.280
7.267
7.251
7.245
7.237
7.233
7.222
7.217
7.192
7.171
6.717
6.696
1.358
0.97
1.04
1.03
3.15
1.14
5.70
1.92
3.16
1.99
1.03
1.04
1.00
1.95
1.04
0.97
1.14
5.70
1.92
3.16
1.99
9.15
f1 (ppm)

IV. ^{13}C NMR spectra of the target molecules in $CDCl_3$

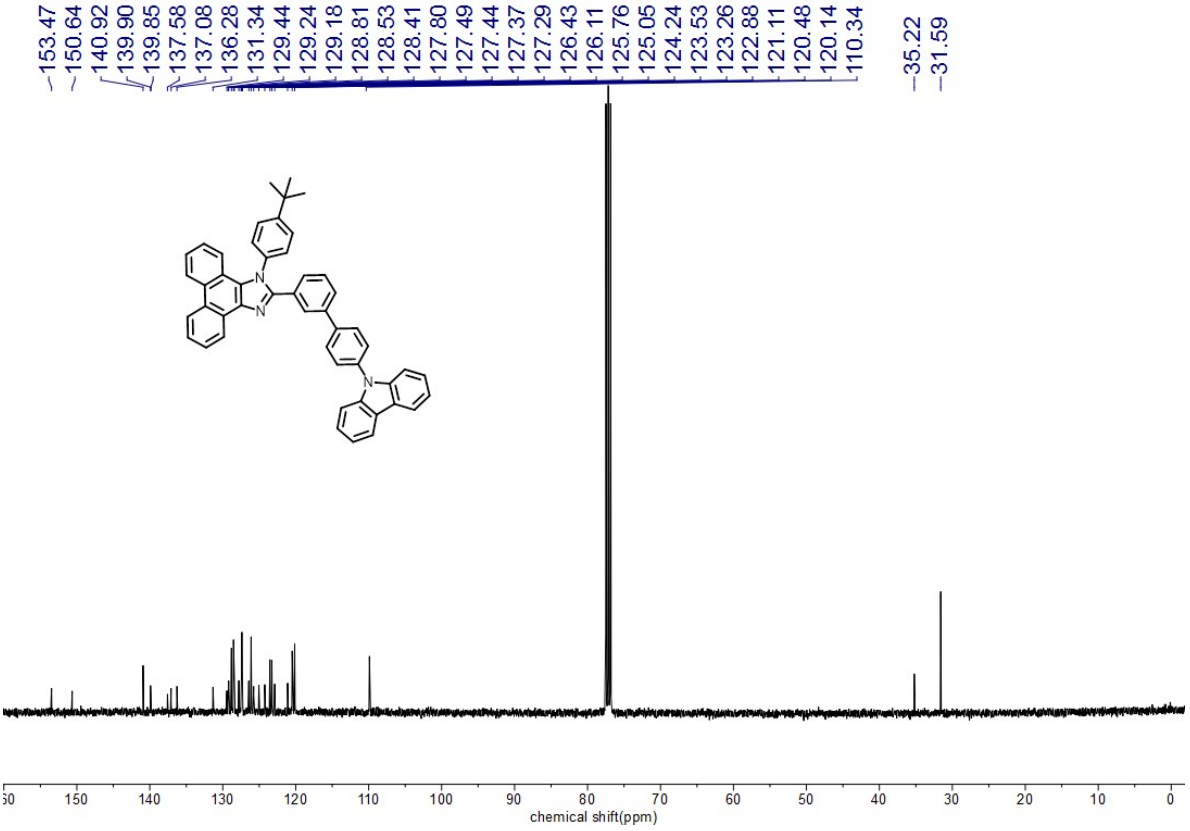

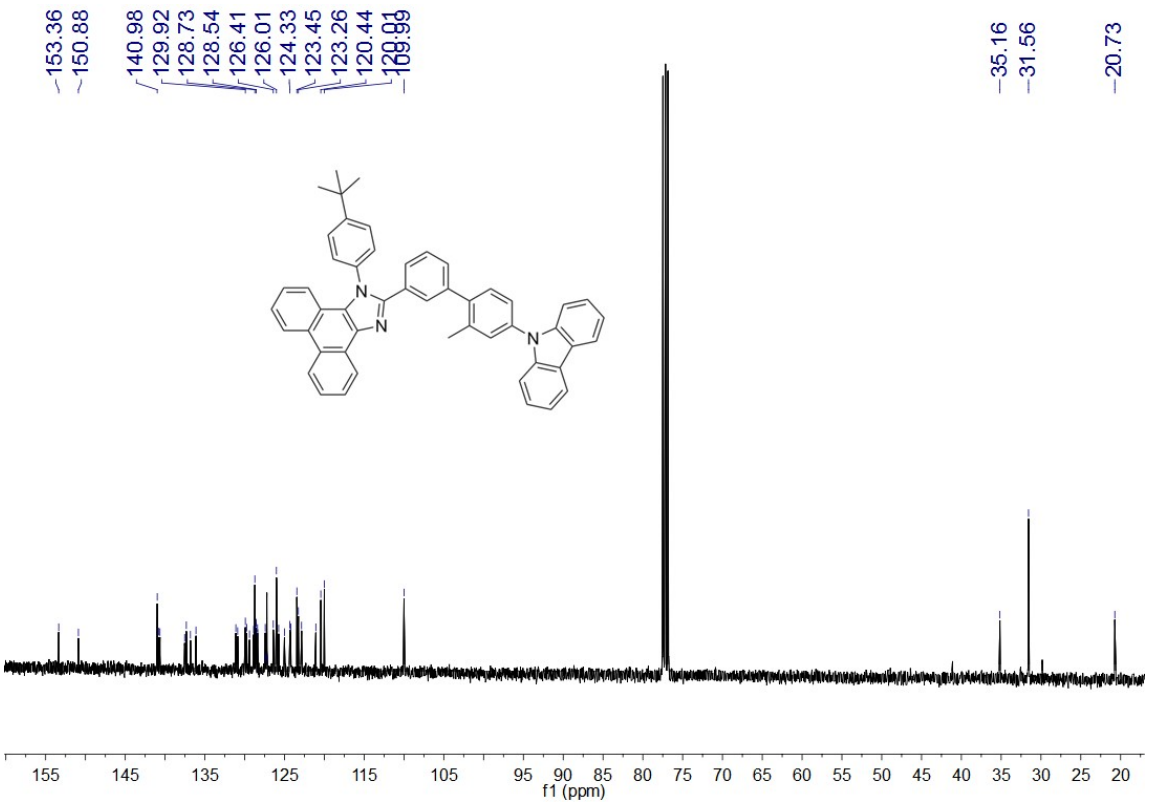

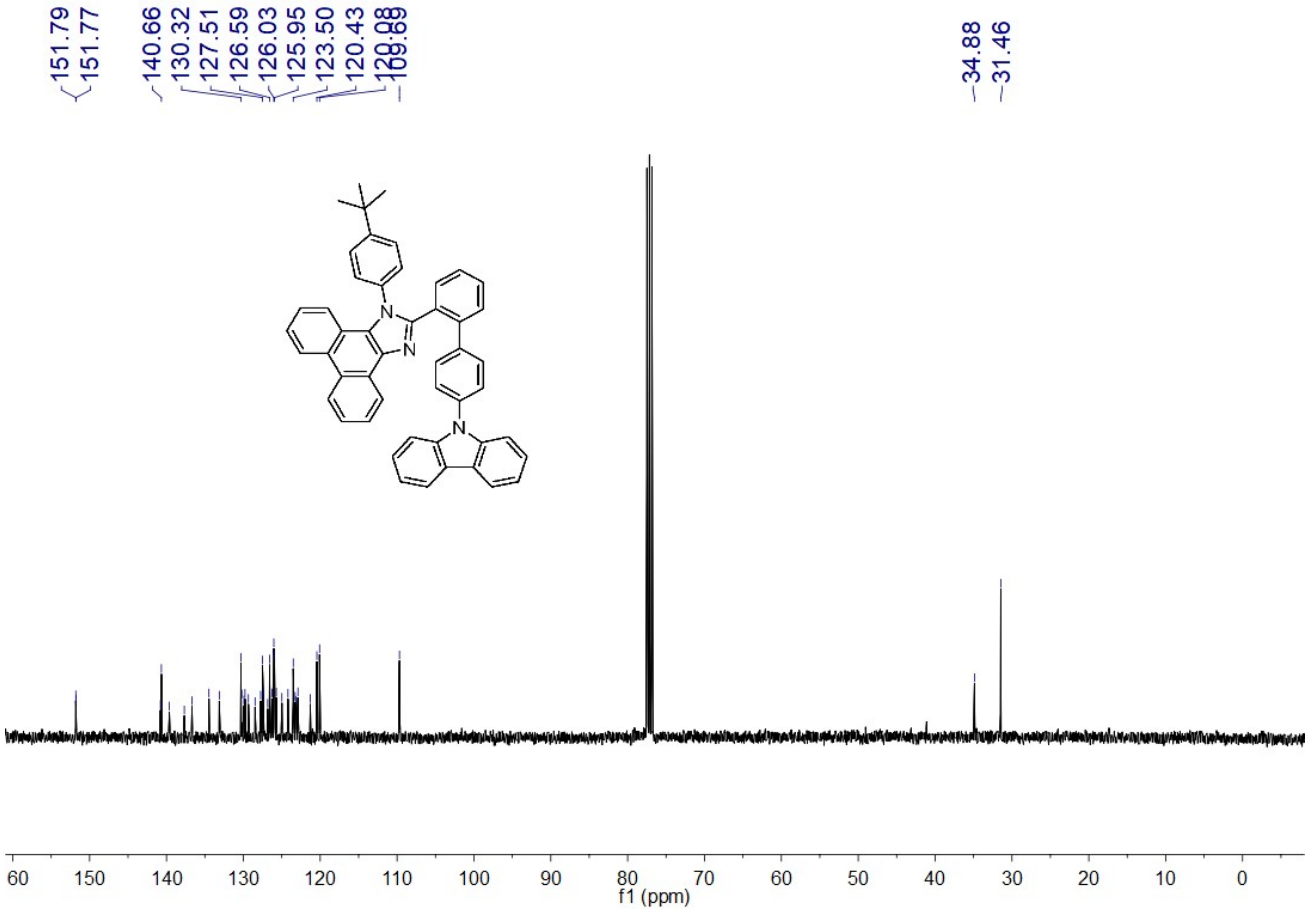
151.79
151.77
140.66
130.32
127.51
126.59
126.03
125.95
123.50
120.43
34.88
31.46
f1 (ppm)

V. HR-MS spectra of the target molecules

Mass Spectrum SmartFormula Report

Analysis Info

Analysis Name	D:\Data\ESITOF-LUH-20211229-LH-WXH-D2_01.d	Acquisition Date	1/5/2022 3:14:51 PM
Method	ESI+100-800-200910.m	Operator	BDAL@DE
Sample Name	Q-TOF-WM-211011-WM-2_01	Instrument / Ser#	microTOF-Q II 228888.10324
Comment			

Acquisition Parameter

Source Type	ESI	Ion Polarity	Positive	Set Nebulizer	1.6 Bar
Focus	Active	Set Capillary	4000 V	Set Dry Heater	220 °C
Scan Begin	100 m/z	Set End Plate Offset	-500 V	Set Dry Gas	4.0 l/min
Scan End	900 m/z	Set Collision Cell RF	200.0 Vpp	Set Divert Valve	Source

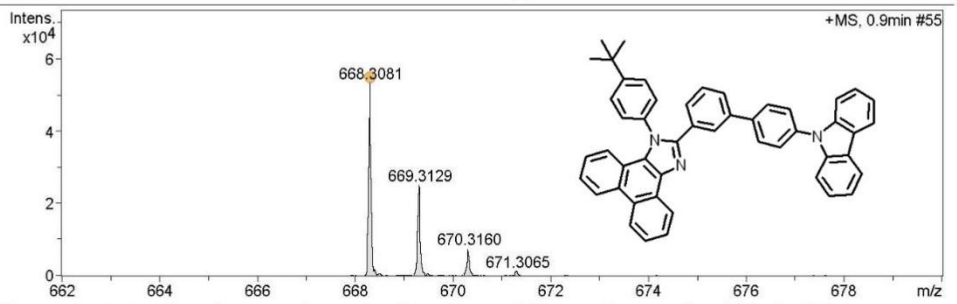

Meas. m/z	#	Ion Formula	m/z	err [ppm]	mSigma	# Sigma	Score	rdb	e⁻ Conf	N-Rule
668.3081	1	C49H38N3	668.3060	-3.1	37.7	4	100.00	32.5	even	ok

Mass Spectrum SmartFormula Report

Analysis Info

Analysis Name	D:\Data\ESITOF-LH-20220704-ZZT-E3-01.d	Acquisition Date	7/14/2022 10:33:54 AM
Method	ESI+100-800-200910.m	Operator	BDAL@DE
Sample Name	Q-TOF-WM-211011-WM-2_01	Instrument / Ser#	microTOF-Q II 228888.10324
Comment			

Acquisition Parameter

Source Type	ESI	Ion Polarity	Positive	Set Nebulizer	1.6 Bar
Focus	Active	Set Capillary	4000 V	Set Dry Heater	200 °C
Scan Begin	100 m/z	Set End Plate Offset	-500 V	Set Dry Gas	4.0 l/min
Scan End	900 m/z	Set Collision Cell RF	200.0 Vpp	Set Divert Valve	Source

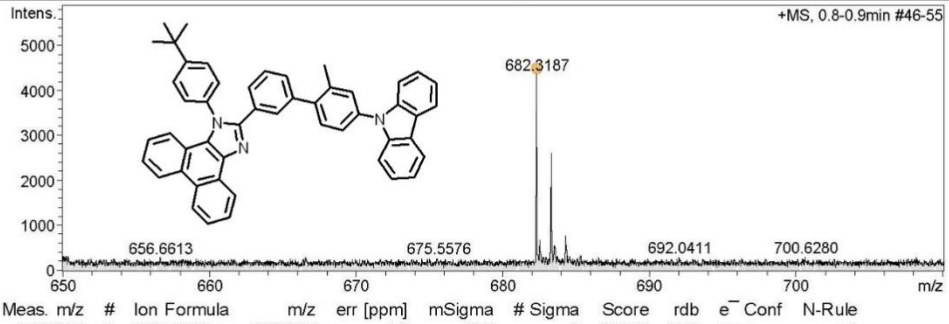

Meas. m/z	#	Ion Formula	m/z	err [ppm]	mSigma	# Sigma	Score	rdb	e⁻ Conf	N-Rule
682.3187	1	C50H40N3	682.3217	4.4	41.7	1	100.00	32.5	even	ok

Mass Spectrum SmartFormula Report

Analysis Info

Analysis Name	D:\Data\ESITOF-LH-20220704-ZZT-E5-01.d	Acquisition Date	7/14/2022 10:36:47 AM
Method	ESI+100-800-200910.m	Operator	BDAL@DE
Sample Name	Q-TOF-WM-211011-WM-2_01	Instrument / Ser#	microTOF-Q II 228888.10324
Comment			

Acquisition Parameter

Source Type	ESI	Ion Polarity	Positive	Set Nebulizer	1.6 Bar
Focus	Active	Set Capillary	4000 V	Set Dry Heater	200 °C
Scan Begin	100 m/z	Set End Plate Offset	-500 V	Set Dry Gas	4.0 l/min
Scan End	900 m/z	Set Collision Cell RF	200.0 Vpp	Set Divert Valve	Source

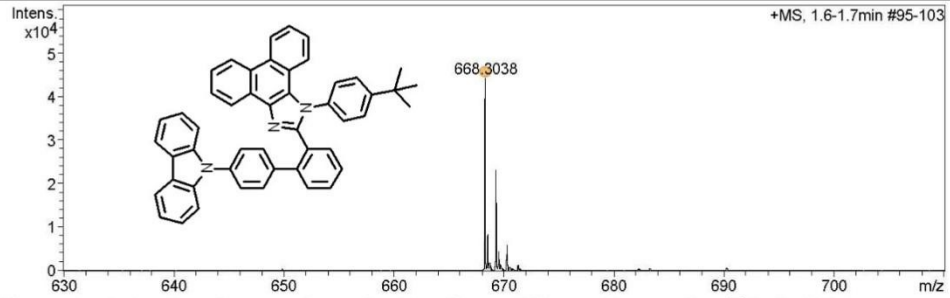

Meas. m/z	#	Ion Formula	m/z	err [ppm]	mSigma	# Sigma	Score	rdb	e⁻ Conf	N-Rule
668.3038	1	C49H38N3	668.3060	-3.3	13.2	1	100.00	32.5	even	ok